Synthesis and Photoelectrochemical Property of Urchin-like Zn/ZnO Core−Shell Structures

Dai-Ming Tang,[†] Gang Liu,[†,‡] Feng Li,[†] Jun Tan,[†] Chang Liu,*[,†] Gao Qing Lu,[‡] and Hui-Ming Cheng[†]

Shenyang National Laboratory for Materials Science, Institute of Metal Research, Chinese Academy of Sciences, 72 Wenhua Road, Shenyang 110016, China, and ARC Centre of Excellence for Functional Nanomaterials, School of Engineering and AIBN, The University of Queensland, Brisbane, Queensland 4072, Australia

Received: December 5, 2008; Revised Manuscript Received: May 13, 2009

An urchin-like Zn/ZnO core−shell structure was synthesized and deposited directly on an indium tin oxide (ITO) glass substrate by using a thermal evaporation method. Structural characterization reveals that the hybrid material is composed of a micrometer scale sphere-shaped metallic Zn core and a shell made up of numerous radially protruding single-crystalline ZnO nanorods. It was found that the Zn core makes direct contact with the ITO layer, which enhances the interface bonding and conductance between the Zn/ZnO structure and the substrate. Desirable photoelectrochemical properties of such Zn/ZnO core−shell structures are demonstrated. Their superior photoelectrical response performance can be attributed to the metal−semiconductor core−shell structure, unique urchin-like configuration, and favorable combination between the active material and the substrate.

Introduction

The design and synthesis of core−shell-structured nanomaterials have attracted intense research interest in recent years,[1−3] because heterojunctions formed at the core−shell interface render interesting physical phenomena and a promising prospect in making functional devices, and multifunctionality and desirable properties can be expected for these multiplex materials with optimized composition and structure. ZnO is a semiconductor with a wide band gap (3.37 eV) and a large excitation binding energy (60 meV), and its promising applications in optoelectronic devices,[4] sensors,[5] solar energy devices,[6] and piezoelectric nanogenerators[7] have been demonstrated or proposed. There have been many studies on the fabrication and properties of ZnO-based core−shell structures, such as ZnO/TiO_2,[8] ZnO/Er_2O_3,[9] Ga_2O_3/ZnO,[10] In_2O_3/ZnO,[11] ZnO/ZnS,[12−15] ZnO/SiC,[16] Ge/ZnO,[17] Co/ZnO,[18] Zn/ZnO,[19−22] and ZnO/polymer[23] in forms of nanocables,[24,25] nanobelts,[20] nanotubes,[10] nanodisks,[19,21] nanohelices,[16] and nanoparticles.[22,23,26] It is demonstrated that a suitable design and precise control of the configuration and chemical composition of ZnO-based core−shell structures can be an efficient way to fabricate hybrid materials with enhanced performance and functionality.

It is known that ZnO and TiO_2 nanostructures are attractive photocatalysts for solar energy conversion with advantages of low cost and relatively high efficiency.[27−30] However, the ZnO and TiO_2 nanoparticle photocatalysts suffer from the problems of quick recombination of photoinduced electron−hole pairs and slow electron transport due to their high density of defects and interfaces, which intrinsically limits the integrated performance of the solar energy conversion devices constructed.[30] Efforts have been made to overcome these disadvantages. For example, Law et al. achieved a direct electron pathway by using crystalline ZnO nanowires as a photoanode,[6] and Hendry et al. reported that the electron mobility of polycrystalline titania nanotubes can be 2 orders of magnitude higher than that of mesoporous nanocrystalline titania.[31] On the other hand, Kamat et al. reported an improved photoinduced charge separation in semiconductor−metal composite nanoclusters.[32] Therefore, it is reasonable to expect that an effective integration of single-crystalline ZnO nanostructures and a metal component would lead to a desirable photoanode material with enhanced charge separation and transport performance.

We report in this paper the fabrication and photoelectrochemical (PEC) property of a novel urchin-like Zn/ZnO core−shell structure. This hybrid material contains a Zn sphere core, and the shell, distinct from all previously reported core−shell structures, whose shells are usually a coaxial layer of the core, is composed of numerous radially protruding single-crystalline ZnO nanorods in this work. The core−shell structure was synthesized by a thermal evaporation method and was deposited directly on an indium tin oxide (ITO) glass substrate, which guarantees a strong adherence and favorable conductance between Zn/ZnO and the substrate. We hypothesize that the single-crystalline ZnO nanorods thus prepared could be a very active photoanode exhibiting rapid carrier transport, and the Zn/ZnO heterostructure enhances the collection and separation of photoinduced charges. We demonstrate very attractive PEC performance of the urchin-like Zn/ZnO core−shell-structured photoanode. In combination with their simple and cost-efficient fabrication process, these Zn/ZnO core−shell structures can be a promising candidate for anode material of solar energy conversion devices.

Experimental Section

Synthesis of the Urchin-like Zn/ZnO Core−Shell Structures. ZnO powder was placed at the center of a horizontal tubular furnace and heated to high temperature (1200−1350 °C) at a rate of 30 °C/min with Ar as the carrier gas. A layer of white product was found deposited on the ITO glass substrate put downstream in the ceramic reactor, where the temperature is examined to be ∼300 °C.

* To whom correspondence should be addressed. E-mail: cliu@imr.ac.cn.
[†] Chinese Academy of Sciences.
[‡] The University of Queensland.

10.1021/jp8107254 CCC: $40.75
Published on Web 06/03/2009

Characterizations. The as-prepared products were characterized by using X-ray diffraction (XRD; Rigaku, RINT 2200, Cu Kα, $\lambda = 1.5406$ Å), scanning electron microscopy (SEM; LEO Supra-35), and transmission electron microscopy (TEM; Tecnai G2 F30). An FIB (focused ion beam; Nova 200, Nanolab) workstation was employed to investigate the morphology and elemental distribution of the inner part of the urchin-like Zn/ZnO structure. The binding energy of the urchin-like Zn/ZnO was identified by X-ray photoelectron spectroscopy with Mg Kα radiation (PHI5300). A UV−vis spectrophotometer (JASCO-550) was used to measure the optical absorption spectra of the material.

Measurements Details of PEC Cells. PEC photocurrent voltage measurements were taken in a standard three-electrode glass cell using a saturated calomel electrode (SCE) as the reference electrode, with an immersed area of 2 cm^2. The electrolyte was 0.1 M Na_2SO_4, and the light source was a Xe lamp with a light intensity of about 150 mW/cm^2. The incident photon-to-current upon monochromatic light, supplied by a computer-controlled monochromator, was measured at a bias of 0.3 V. The incident photon-to-current efficiency (IPCE) for each wavelength was calculated from the photocurrent density according to

$$\text{IPCE}\ (\%) = 1240I/P\lambda \times 100 \quad (1)$$

where I is the photocurrent density (mA/cm^2), P is the light power density (mW/cm^2), and λ is the incident light wavelength (nm).

Results and Discussion

Parts a and b of Figure 1 show SEM images of the as-prepared products with different magnifications. A compact layer of particles is deposited uniformly on the ITO glass substrate (Figure 1a), and the particles have an urchin-like structure with a diameter in the range of 10−20 μm (Figure 1b). We can see under higher magnification that each "urchin" is composed of numerous nanorods protruding radially from the center (inset of Figure 1b). The mean diameter of the nanorods is about 100 nm, and each nanorod has a hexagonal cross section. The interspace between the nanorods varies from the central part to the periphery part of the urchin in the range of several nanometers to hundreds of nanometers due to the unique radial configuration, and micrometer scale pores exist between the urchins.

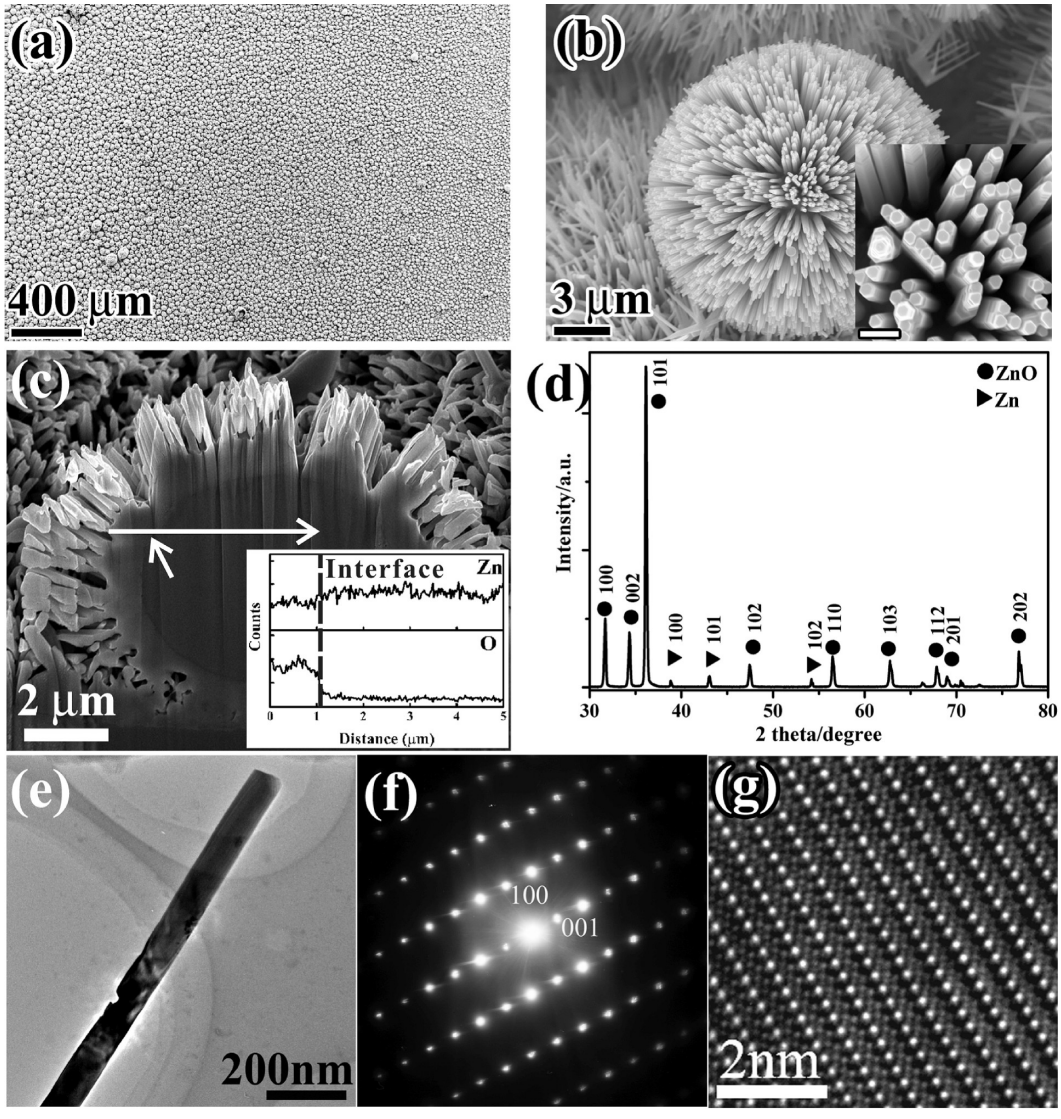

Figure 1. Low-magnification (a) and higher magnification (b) SEM images of the urchin-like Zn/ZnO structures. (c) SEM image of the cross section of a Zn/ZnO "urchin". Inset: results of Zn and O elemental line-scan analysis along the long arrow. (d) XRD spectrum of the urchin-like Zn/ZnO structures. TEM images (e, g) and SAED pattern (f) of a ZnO nanorod. Scale bar in the inset of (b): 400 nm.

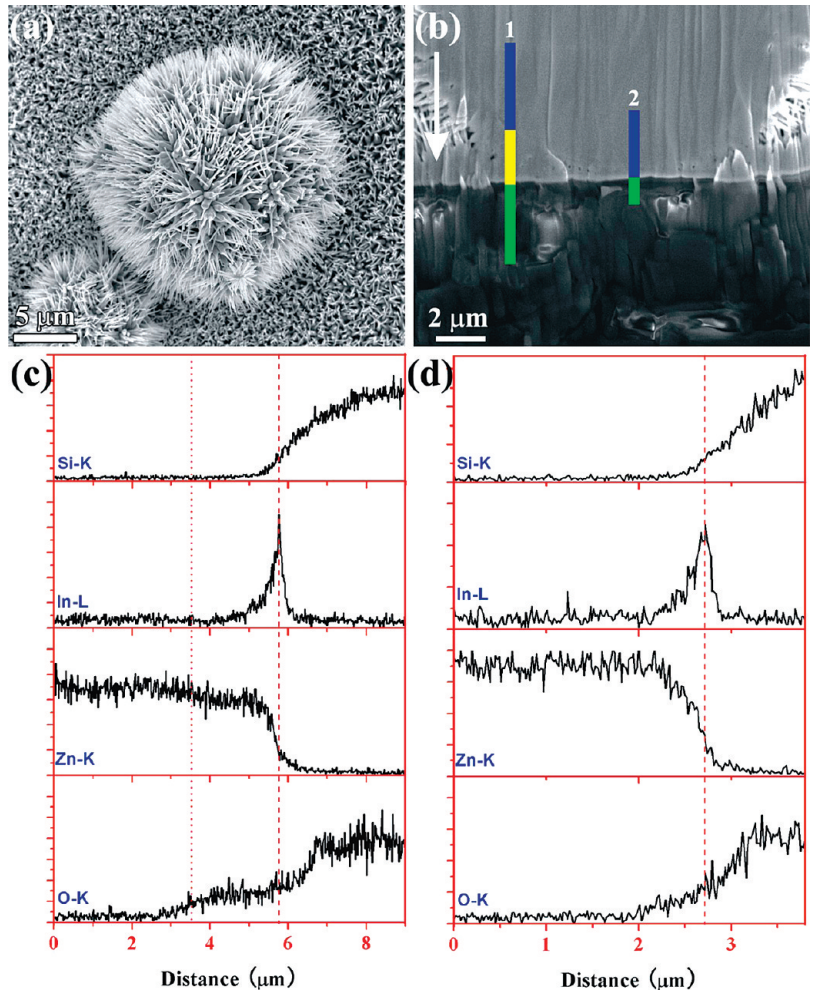

Figure 2. SEM image of a Zn/ZnO urchin (a) and the interface (b) between the cut urchin and the substrate. Results of elemental line-scan analysis along lines 1 (c) and 2 (d) labeled in (b) for the elements of Si, In, Zn, and O.

To reveal the inner structure of the urchin, an FIB was employed to cut the urchin open and to investigate its morphology and composition. Figure 1c shows a typical secondary electron FIB image of the cross section of a cut urchin. A distinct change in contrast, as indicated with the short arrow, can be observed. The result of elemental line-scan analysis of Zn and O along the radial direction (indicated with the long arrow) shown in the inset of Figure 1c reveals that the urchin is composed of a pure Zn core, a ZnO outer layer, and a ZnO nanorod array. The above-mentioned contrast change is due to the Zn/ZnO interface. XRD was used to analyze the phase composition of the product. The pattern (Figure 1d) can be indexed as a ZnO phase (PDF standard card 36-1451) and a Zn phase (PDF standard card 04-0831), which is consistent with the above elemental analysis results. Parts e−g of Figure 1 present the typical TEM images and selected area electron diffraction (SAED) pattern of a ZnO nanorod. We can see that the nanorod is straight, and no amorphous layer can be observed on its surface. SAED analysis and TEM observations show that the nanorod is single-crystalline wurtzite phase ZnO, and the growth direction is along [0002].

The interface between the Zn/ZnO urchin and the ITO glass substrate is important for charge transfer and may influence the photoelectrochemical property of the Zn/ZnO urchins. Therefore, FIB is employed to reveal the morphology and elemental distributions at the interface. Figure 2a is an SEM image of an original Zn/ZnO urchin. Figure 2b shows the interface between the cut Zn/ZnO urchin and the ITO glass substrate. We can see from Figure 2b that the Zn/ZnO urchin contacts well with the substrate. On the basis of the sectional image observations, the thickness of the deposited film is determined to be 10−15 μm, slightly smaller than the mean diameter of the urchins. Elemental line-scan analysis along lines 1 and 2 labeled in Figure 2b were performed, and the results are shown in parts c and d, respectively, of Figure 2. For line 1, there are two distinct compositional steps, indicating that Zn, ZnO, and ITO glass exist along the line, while, for line 2, there is only one compositional step, indicating the existence of Zn and ITO glass. An increased oxygen platform and a decreased zinc platform appear in Figure 2c, corresponding to the transformation of the pure Zn core to the outer ZnO layer along line 1. While in Figure 2d no such platforms can be observed, the slightly increased oxygen signal at the interface can be attributed to the ITO and SiO_2 phases of the substrate. Combining the results of SEM observations and elemental line-scan analysis, we conclude that the Zn core of the Zn/ZnO urchin contacts directly with the ITO glass.

The composition and chemical states of the as-prepared sample were further investigated by X-ray photoelectron spectroscopy (XPS) analysis. Figure 3 shows the high-resolution XPS spectra for the O 1s (a) and Zn 2p (b) regions. The binding energies of Zn $2p_{3/2}$ and Zn $2p_{1/2}$ are 1020.1 and 1043.7 eV, respectively, and the O 1s peak is centered at 530.3 eV, which agrees well with the reported values for ZnO.[33] Therefore, it is

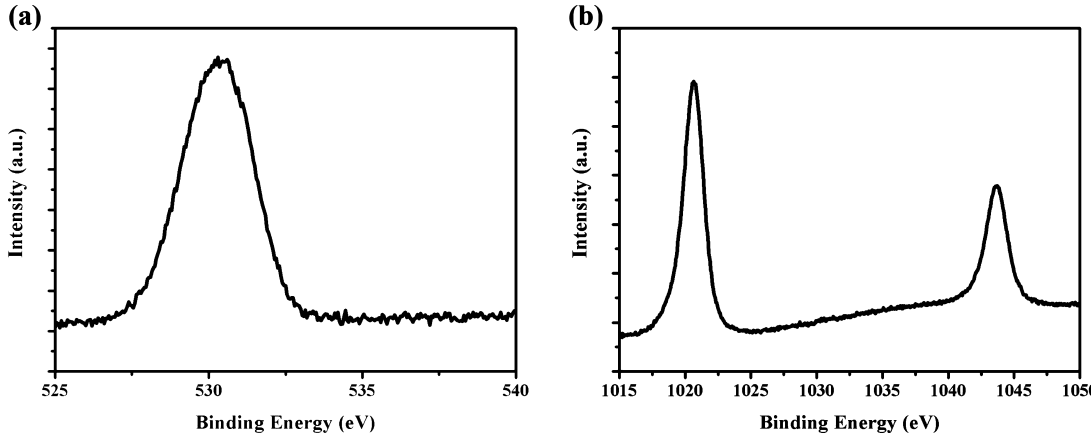

Figure 3. XPS spectra of the as-prepared Zn/ZnO structure: (a) O 1s spectrum, (b) Zn 2p spectrum.

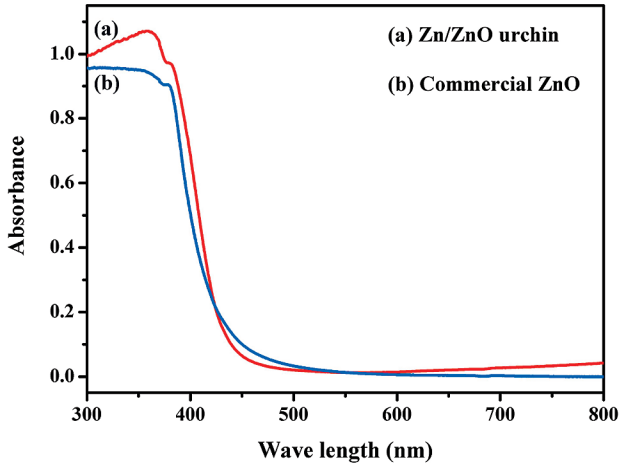

Figure 4. UV−vis absorption spectra of the Zn/ZnO urchins (a, red) and commercially available ZnO (b, blue) as a reference.

further confirmed that the surface of the material is composed of ZnO, consistent with the elemental analysis results by FIB.

Figure 4 shows the optical absorption spectra of the Zn/ZnO urchins (a) and that of a commercially available ZnO sample (b) for reference. No distinct difference can be observed between the spectra; an absorption edge located at 3.04−3.24 eV appears for both samples. However, the Zn/ZnO urchin sample shows a slight increase in the absorbance in the longer wavelength range (550−800 nm), which is usually observed for metal/metal oxide composites[34] and could be ascribed to the absorption of the metallic Zn core in this study.

On the basis of the above structural characterizations, we know that the urchin-like structures are composed of a Zn core, a ZnO outer layer, and a protruding ZnO nanorod array, and the Zn core contacts directly with the ITO substrate. These materials were synthesized by a thermal evaporation method using ZnO powder as the starting material and Ar as the carrier gas under ambient pressure. The ZnO powder was vaporized at high temperature, and the ITO glass substrate for product collection was located downstream at a temperature of ∼300 °C. Here we propose the growth process of these Zn/ZnO core−shell structures as follows: First, the ZnO powder is vaporized and decomposed into zinc and oxygen at a high temperature. Then the zinc vapor is transported by the carrier gas to the lower temperature zone (∼300 °C), where they condense to form liquid droplets and then solid spheres on the substrate surface (the melting point of Zn is 419.6 °C). Subsequently, the zinc spheres are oxidized by oxygen and a layer of ZnO formed on their surface. Next nucleus sites gradually form on the sphere surface due to a large lattice mismatch in the basal plane (0002) between Zn and ZnO, and small ZnO nanorods sprout out epitaxially from the surface via a self-catalytic mechanism. The nanorods keep growing until the feeding of zinc and oxygen ceases, and an urchin-like Zn/ZnO structure forms. A schematic diagram illuminating the above growth process is shown in Scheme 1.

Shen et al. reported a hollow ZnO urchin synthesized by a thermal evaporation method with Zn as the raw material.[35] The growth process included the vaporization of Zn powder, condensation of Zn liquid droplets, surface oxidation, sublimation of the Zn core, and growth of ZnO nanowires. Gao et al. studied the influences of the experimental conditions on the growth of Zn/ZnO core−shell nanostructures.[19] It was found that the oxidation and growth temperature and the pressure control the growth kinetics and the final morphologies. In our study, besides the urchin-like Zn/ZnO structures, ZnO particles and ZnO nanowire arrays can be synthesized by tuning the growth conditions such as the amount of raw materials and the gas flow rate of the carrier gas (see the experimental details and SEM images in the Supporting Information).

To gain some perspective on the solar energy conversion performance of the urchin-like Zn/ZnO structure, its photoelectrocurrent property was studied. Instead of Si substrates which are commonly used for the deposition of ZnO nanostructures,[20,35] ITO glasses are employed in this work for collecting the products to achieve a desirable adhesion and conductance between the sample and the substrate. ZnO nanowire arrays (Figure S1c, Supporting Information) and TiO_2 nanotube arrays (Figure S2, Supporting Information), both of which were recently found to display very good PEC properties,[6,36,37] were also tested under identical conditions for comparison purpose. Figure 5a presents the applied voltage dependence of the photocurrent densities of the photoanode materials under the irradiation of a Xe lamp. The turn-on potential of the photocurrent for the Zn/ZnO urchins is about −0.21 V, similar to that of TiO_2 nanotube arrays, which is attributed to the comparable electronic structures of ZnO and TiO_2 (anatase phase). With an increase of the applied potential, the photocurrent density of the urchin-like Zn/ZnO anode keeps increasing and reaches 0.88 mA/cm^2 at an applied potential of 1.0 V, much higher than those of the ZnO nanowire array and TiO_2 nanotube array anodes. In addition, the IPCEs of the Zn/ZnO urchin and the TiO_2 nanotube array were tested for comparison, and the resulting curves are shown in Figure S3, Supporting Information.

SCHEME 1: Growth Process of the Urchin-like Zn/ZnO Structures[a]

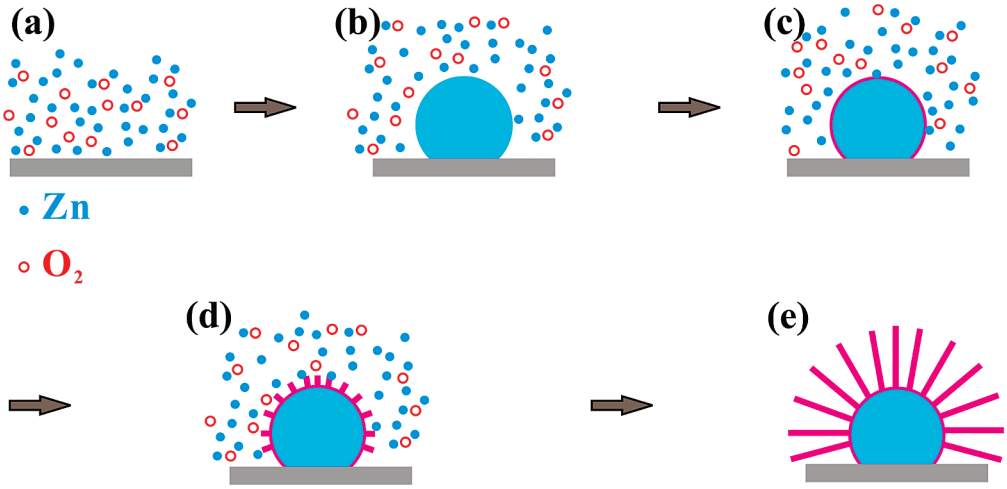

[a] Small blue solid and red hollow spheres represent zinc vapor and oxygen, respectively. The process involves the vaporization and decomposition of ZnO, transportation of Zn vapors to the lower temperature zone (a), condensation and formation of a Zn liquid droplet on an ITO glass substrate (b), solidification and surface oxidation of Zn spheres (c), epitaxial nucleation and growth of ZnO nanorods from the oxidized layer (d), further growth of ZnO nanorods, and finally the formation of urchin-like Zn/ZnO structures (e).

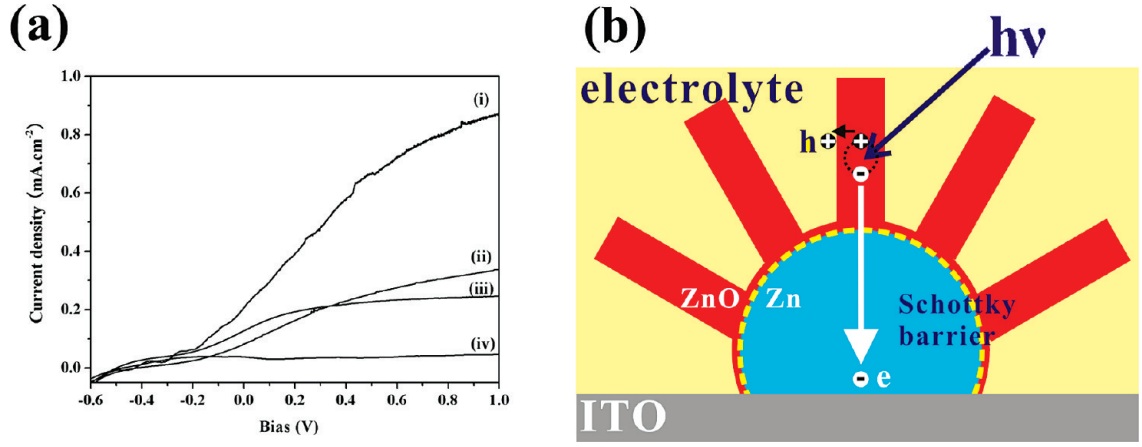

Figure 5. (a) Voltage dependence of the photocurrent density versus saturated calomel electrode for the urchin-like Zn/ZnO structures (i), ZnO nanowire arrays (ii), and TiO_2 nanotube arrays (iii) under the irradiation of a 75 W Xe lamp. The result obtained in the dark for the urchin-like Zn/ZnO structure is also shown (iv) for reference. (b) A schematic diagram showing the generation, separation, and transport of the photoinduced charges in an urchin-like Zn/ZnO core−shell structure.

We can see that the IPCE of the Zn/ZnO urchin is much higher than that of the TiO_2 nanotube arrays, in accordance with the PEC results.

The outstanding PEC performance of the Zn/ZnO urchin anodes is related to their unique structure. A schematic diagram showing the generation, separation, and transport of the photoinduced charges in an urchin-like Zn/ZnO core−shell structure is shown in Figure 5b. Upon photoexcitation, electron−hole pairs are generated in the ZnO nanorods. Holes diffuse through the radial direction to the surface of the ZnO nanorod to meet the electrolyte, and the electrons diffuse along the axis direction of the ZnO nanorod to the ZnO/Zn interface, the Zn core, and finally the ITO substrate. The above process is quite different from those of nanoparticle-based and nanotube-based photoanodes, and the advantages of our novel Zn/ZnO core−shell structure are proposed as follows. First, the single-crystalline ZnO can provide direct channels for electron transport, drastically increasing the charge diffusion length and reducing the rate of recombination.[6] The diameter of the ZnO nanorods is about 100 nm, and the diameter and tube wall thickness of the TiO_2 nanotubes are about 80 and 10 nm, respectively. While the photocurrent density of the TiO_2 nanotubes is limited by the tube wall thickness,[37] the ZnO nanorods can supply a sufficient space charge layer even at a high applied potential. Therefore, a higher photocurrent density is achieved for the Zn/ZnO core−shell structures. Second, a Schottky barrier may form at the Zn/ZnO interface due to their different work functions.[38] Upon photon excitation, the metal core can act as an electron sink, and the photoinduced electrons in the ZnO nanorods are apt to transport through the ZnO/Zn interface to the Zn core. Third, the Zn/ZnO structure is deposited directly onto the ITO glass substrate with the Zn core in contact directly with the ITO layer by thermal evaporation; hence, a good adherence and efficient electron transfer between the photoanode and the substrate can be guaranteed. In addition, each of the urchin-like units consists of numerous radially protruding ZnO nanorods that form a 3-D network. Interspaces ranging from several nanometers to hundreds of nanometers coexist in the Zn/ZnO core−shell structure due to their unique urchin-like configuration. These hierarchical pores may facilitate the ion transport in elec-

trolyte.[39] Therefore, the enhanced PEC performance can be attributed to the improved photoinduced charge separation and transport, arising from the structural characteristics of the urchin-like Zn/ZnO core−shell structures.

Conclusions

In summary, a novel urchin-like Zn/ZnO core−shell structure was prepared via a simple thermal vaporization method. Distinct from the previously reported core−shell structures, whose shells are usually a coaxial layer of the core, we synthesized an urchin-like core−shell structure composed of single-crystalline ZnO nanorods radially protruding from the central Zn core. Such a Zn/ZnO core−shell structure exhibited a superior photoelectrical response property compared to ZnO nanowire arrays and TiO_2 nanotube arrays. The outstanding PEC performance of the Zn/ZnO core−shell structure can be attributed to its metal−semiconductor core−shell structure, unique urchin-like configuration, and favorable combination with the substrate. Considering their simple, cost-efficient fabrication process, these Zn/ZnO core−shell structures can be a promising candidate for anode material in solar energy conversion devices.

Acknowledgment. This work is supported by the Chinese Academy of Sciences and the Ministry of Science and Technology of China (Grant No. 2009CB220001). We acknowledge the kind help from Prof. Q. B. Meng.

Supporting Information Available: Typical growth conditions for the Zn/ZnO urchins, ZnO nanowire arrays, and ZnO particles, SEM images of the ZnO particles and ZnO nanowire arrays, SEM image and XRD spectrum of the TiO_2 nanotube arrays, and IPCE spectra of urchin-like Zn/ZnO core−shell structures and TiO_2 nanotube arrays. This material is available free of charge via the Internet at http://pubs.acs.org.

References and Notes

(1) Wu, Y. Y.; Fan, R.; Yang, P. D. *Nano Lett.* **2002**, *2*, 83–86.
(2) Jiao, J.; Seraphin, S.; Wang, X. K.; Withers, J. C. *J. Appl. Phys.* **1996**, *80*, 103–108.
(3) Consonni, M.; Jokic, D.; Murzin, D. Y.; Touroude, R. *J. Catal.* **1999**, *188*, 165–175.
(4) Huang, M. H.; Mao, S.; Feick, H.; Yan, H. Q.; Wu, Y. Y.; Kind, H.; Weber, E.; Russo, R.; Yang, P. D. *Science* **2001**, *292*, 1897–1899.
(5) Wang, X. D.; Summers, C. J.; Wang, Z. L. *Nano Lett.* **2004**, *4*, 423–426.
(6) Law, M.; Greene, L. E.; Johnson, J. C.; Saykally, R.; Yang, P. D. *Nat. Mater.* **2005**, *4*, 455–459.
(7) Wang, Z. L.; Song, J. H. *Science* **2006**, *312*, 242–246.
(8) Law, M.; Greene, L. E.; Radenovic, A.; Kuykendall, T.; Liphardt, J.; Yang, P. D. *J. Phys. Chem. B* **2006**, *110*, 22652–22663.
(9) Li, S. Z.; Gan, C. L.; Cai, H.; Yuan, C. L.; Guo, J.; Lee, P. S.; Ma, J. *Appl. Phys. Lett.* **2007**, *90*, 263106.
(10) Hu, J. Q.; Bando, Y.; Liu, Z. W. *Adv. Mater.* **2003**, *15*, 1000–1003.
(11) Lao, J. Y.; Wen, J. G.; Ren, Z. F. *Nano Lett.* **2002**, *2*, 1287–1291.
(12) Li, J. H.; Zhao, D. X.; Meng, X. Q.; Zhang, Z. Z.; Zhang, J. Y.; Shen, D. Z.; Lu, Y. M.; Fan, X. W. *J. Phys. Chem. B* **2006**, *110*, 14685–14687.
(13) Panda, S. K.; Dev, A.; Chaudhuri, S. *J. Phys. Chem. C* **2007**, *111*, 5039–5043.
(14) Schrier, J.; Demchenko, D. O.; Wang, L. W. *Nano Lett.* **2007**, *7*, 2377–2382.
(15) Lin, Y. F.; Hsu, Y. J.; Lu, S. Y.; Chiang, W. S. *Nanotechnology* **2006**, *17*, 4773–4782.
(16) Zhou, J.; Liu, J.; Yang, R. S.; Lao, C. S.; Gao, P. X.; Tummala, R.; Xu, N. S.; Wang, Z. L. *Small* **2006**, *2*, 1344–1347.
(17) Yin, L. W.; Li, M. S.; Bando, Y.; Golberg, D.; Yuan, X. L.; Sekiguchi, T. *Adv. Funct. Mater.* **2007**, *17*, 270–276.
(18) Wei, T.; Jin, C. Q.; Zhong, W.; Liu, J. M. *Appl. Phys. Lett.* **2007**, *91*, 222907.
(19) Gao, P. X.; Lao, C. S.; Ding, Y.; Wang, Z. L. *Adv. Funct. Mater.* **2006**, *16*, 53–62.
(20) Kong, X. Y.; Ding, Y.; Wang, Z. L. *J. Phys. Chem. B* **2004**, *108*, 570–574.
(21) Zhang, X. Y.; Dai, J. Y.; Lam, C. H.; Wang, H. T.; Webley, P. A.; Li, Q.; Ong, H. C. *Acta Mater.* **2007**, *55*, 5039–5044.
(22) Zeng, H. B.; Cai, W. P.; Cao, B. Q.; Hu, J. L.; Li, Y.; Liu, P. S. *Appl. Phys. Lett.* **2006**, *88*, 181905.
(23) Xiong, H. M.; Wang, Z. D.; Xia, Y. Y. *Adv. Mater.* **2006**, *18*, 748–751.
(24) Hu, J. Q.; Li, Q.; Meng, X. M.; Lee, C. S.; Lee, S. T. *Chem. Mater.* **2003**, *15*, 305–308.
(25) Wong, Y. H.; Li, Q. *J. Mater. Chem.* **2004**, *14*, 1413–1418.
(26) Ren, F.; Guo, L. P.; Shi, Y.; Chen, D. L.; Wu, Z. Y.; Jiang, C. Z. *J. Phys. D: Appl. Phys.* **2006**, *39*, 488–491.
(27) Fujishima, A.; Honda, K. *Nature* **1972**, *238*, 37–38.
(28) Grätzel, M. *Nature* **2001**, *414*, 338–344.
(29) Grätzel, M. *J. Photochem. Photobiol., C: Photochem. Rev.* **2003**, *4*, 145–153.
(30) Beek, W. J. E.; Wienk, M. M.; Janssen, R. A. J. *Adv. Mater.* **2004**, *16*, 1009–1013.
(31) Hendry, E.; Koeberg, M.; O'Regan, B.; Bonn, M. *Nano Lett.* **2006**, *6*, 755–759.
(32) Kamat, P. V.; Shanghavi, B. *J. Phys. Chem. B* **1997**, *101*, 7675–7679.
(33) Xu, C. K.; Xu, G. D.; Liu, Y. K.; Wang, G. H. *Solid State Commun.* **2002**, *122*, 175–179.
(34) Pal, U.; Garcia-Serrano, J.; Casarrubias-Segura, G.; Koshizaki, N.; Sasaki, T.; Terahuchi, S. *Sol. Energy Mater. Sol. Cells* **2004**, *81*, 339–348.
(35) Shen, G. Z.; Bando, Y.; Lee, C. J. *J. Phys. Chem. B* **2005**, *109*, 10578–10583.
(36) Mor, G. K.; Shankar, K.; Paulose, M.; Varghese, O. K.; Grimes, C. A. *Nano Lett.* **2005**, *5*, 191–195.
(37) Beranek, R.; Tsuchiya, H.; Sugishima, T.; Macak, J. M.; Taveira, L.; Fujimoto, S.; Kisch, H.; Schmuki, P. *Appl. Phys. Lett.* **2005**, *87*, 243114.
(38) Fonash, S. J. *J. Appl. Phys.* **1975**, *46*, 1286–1289.
(39) Kakiuchi, K.; Hosono, E.; Fujihara, S. *J. Photochem. Photobiol., A* **2006**, *179*, 81–86.

JP8107254